Carcinogenesis vol.29 no.12 pp.2306–2316, 2008
doi:10.1093/carcin/bgn231
Advance Access publication October 8, 2008

Impaired DNA double-strand break repair contributes to chemoresistance in HIF-1α-deficient mouse embryonic fibroblasts

Renato Wirthner, Simon Wrann, Kuppusamy Balamurugan, Roland H.Wenger* and Daniel P.Stiehl

Institute of Physiology and Zürich Center for Integrative Human Physiology, University of Zürich, Winterthurerstrasse 190, CH-8057 Zürich, Switzerland

*To whom correspondence should be addressed. Tel: +41 44 6355065; Fax: +41 44 6356814;
Email: roland.wenger@access.uzh.ch

A mismatch between metabolic demand and oxygen delivery leads to microenvironmental changes in solid tumors. The resulting tumor hypoxia is associated with malignant progression, therapy resistance and poor prognosis. However, the molecular mechanisms underlying therapy resistance in hypoxic tumors are not fully understood. The hypoxia-inducible factor (HIF) is a master transcriptional activator of oxygen-regulated gene expression. Transformed mouse embryonic fibroblasts (MEFs) derived from HIF-1α-deficient mice are a popular model to study HIF function in tumor progression. We previously found increased chemotherapy and irradiation susceptibility in the absence of HIF-1α. Here, we show by single-cell electrophoresis, histone 2AX phosphorylation and nuclear foci formation of γH2AX and 53BP1, that the number of DNA double-strand breaks (DSB) is increased in untreated and etoposide-treated HIF-deficient MEFs. In etoposide-treated cells, cell cycle control and p53-dependent gene expression were not affected by the absence of HIF-1α. Using a candidate gene approach to screen 17 genes involved in DNA repair, messenger RNA (mRNA) and protein of three members of the DNA-dependent protein kinase complex were found to be decreased in HIF-deficient MEFs. Of note, residual HIF-1α protein in cancer cells with a partial HIF-1α mRNA knockdown was sufficient to confer chemoresistance. In summary, these data establish a novel molecular link between HIF and DNA DSB repair. We suggest that selection of early, non-hypoxic tumor cells expressing low levels of HIF-1α might contribute to HIF-dependent tumor therapy resistance.

Introduction

Due to inadequate vascularization, irregular blood flow, high oxygen consumption and sometimes anemia, solid tumors build up hypoxic areas, resulting in distinct tumor cell phenotypes. Tumor hypoxia is associated with malignant progression, increased metastasis, genetic instability, chemoresistance, radioresistance and poor prognosis (1–3). Therefore, understanding the molecular pathways induced by hypoxia in tumor cells became a major focus in the development of new strategies to improve cancer therapy efficiency.

Central to the physiological response to hypoxia is the oxygen-labile α subunit of the hypoxia-inducible factor (HIF)-1 (4,5). HIF-1 activates a large number of oxygen-regulated genes required for the adaptation of normal cells to hypoxia (6). In cancer, HIF-1 is responsible for vascular endothelial growth factor-dependent tumor angiogenesis, for carbonic anhydrase IX-dependent pH regulation and for the normoxically increased glycolytic capacity of cancer cells, known as Warburg effect (7–9). Likewise, increased HIF activity in hypoxic tumor areas facilitates the switch to anaerobic fermentation (Pasteur effect), allowing cells to maintain metabolic functions even in the absence of oxygen (10). Thus, HIF-1 mediates many of the adverse effects of tumor hypoxia and is an established positive factor for tumor growth (11,12). Apart from tumor hypoxia stabilizing the HIF-1α protein, HIF-1 can be upregulated constitutively due to the loss of tumor suppressors such as pVHL, PTEN and p53 or oncogenes such as v-*src* (13–16). Indeed, HIF is overexpressed in the majority of human cancers with expression levels correlating with malignancy and negative survival prognosis (17–19).

High HIF-1α expression levels in human cancers are also associated with incomplete responses to chemotherapy and radiotherapy (19–22). However, the precise molecular mechanisms underlying hypoxic cancer therapy resistance are not fully understood. One of the first reported molecular mechanisms explaining the involvement of HIF-1 in chemotherapy resistance was the observation that HIF-1 can augment multidrug resistance 1 gene expression (23,24). However, multidrug resistance 1 is not induced in all therapy-resistant cancers and is not involved in hypoxic radioresistance. Hypoxically dysregulated apoptosis in response to chemotherapy might be another explanation (25,26), but the cell type-specific role for HIF-1 in apoptosis is not well established because cells do not undergo apoptosis under degrees of hypoxia sufficient for HIF-1 induction (27).

Resistance to radiotherapy is generally attributed to lowered generation of oxygen-dependent radical formation, at least under severe hypoxic conditions, below the oxygen partial pressure required to induce HIF-1 (28). However, we previously reported that transformed mouse embryonic fibroblasts (MEFs) were more sensitive to chemotherapy as well as to radiotherapy in the absence of HIF-1α (29). Experimental tumors using these cells were also more susceptible to chemotherapy when HIF-1α was absent. These data were supported by a large number of studies that showed reversal of chemoresistance as well as radioresistance by targeting HIF-1 (30–37). On the other hand, experimentally increasing HIF-1α enhanced therapy resistance (38,39). Because HIF-1-mediated therapy resistance was only observed when DNA double-strand break-inducing (DSB) but not single-strand break-inducing treatments were applied, we suspected that HIF-1 might be involved in DNA DSB repair (29). Therefore, we further characterized this putative novel role of HIF-1 in DNA damage and repair.

Abbreviations: ATM, ataxia telangiectasia mutated; DNA-PK, DNA-dependent protein kinase; DSB, double-strand breaks; GADD, growth arrest and DNA damage; HIF, hypoxia-inducible factor; MEF, mouse embryonic fibroblast; mRNA, messenger RNA; PBS, phosphate-buffered saline; PHD, prolyl-4-hydroxylase domain; qPCR, quantitative polymerase chain reaction; RT, reverse transcription; siRNA, small interfering RNA.

Materials and methods

Cell culture

MEF-*Hif1a*$^{+/+}$ and MEF-*Hif1a*$^{-/-}$ cell lines were derived from day 9.5 embryos, either wild-type (*Hif1a*$^{+/+}$) or deficient (*Hif1a*$^{-/-}$) for HIF-1α. MEF cells obtained from independent mouse strains were either transformed with H-*ras* and immortalized with SV40 large T antigen (7,12), herein after referred to as *r*T (kindly provided by R.S.Johnson, La Jolla, CA), or immortalized with SV40 large T antigen alone (40), referred to as T (kindly provided by G.L.Semenza, Baltimore, MD). All cell lines were cultured in Dulbecco's modified Eagle's medium (high glucose) as described previously (41). For long-term hypoxia (up to 256 h), MEFs were grown and passaged in a gas-controlled glove box to handle the cells under constant oxygen (InvivO$_2$ 400, Ruskinn Technologies, Leeds, UK). Cells were grown on 145 mm culture dishes and split every 48 h. Reagents used for splitting and permanent culturing were pre-equilibrated to the oxygen concentration in the glove box. Viability assays were performed with 3-(4,5-dimethylthiazol-2-yl)-2,5-diphenyl tetrazolium bromide as described previously (29).

Colony formation assays

Cells (1×10^6) were cultured on 150 mm tissue culture plates for 24 h and subsequently treated with 1, 2.5 or 5 μM etoposide (Sigma, Buchs, Switzerland) for 60 min. Cells were then trypsinized and counted using a ViCell cell viability analyzer (Beckman-Coulter, Krefeld, Germany). The cells (500–1000) were seeded in triplicates on 100 mm culture plates and grown for an additional 6 days. Following fixation with 2% paraformaldehyde in phosphate-buffered saline (PBS), the colonies were stained with crystal violet,

counted and the numbers normalized to the untreated control groups. The total cell area per 100 mm plate was determined by processing 8-bit binary images using ImageJ software (http://rsb.info.nih.gov/ij/).

Indirect immunofluorescence

MEFs (5×10^4 cells) were seeded on 24-well Lumox plates (Greiner, Frickenhausen, Germany) and treated with etoposide for 1 h. Cells were rinsed with PBS and fixed with 2% paraformaldehyde in PBS for 5 min at room temperature, followed by permeabilization with 100% methanol at −30°C for 5 min. After blocking with 3% bovine serum albumin for 1 h, the primary antibodies rabbit anti-53BP1 (Novus Biologicals, Littleton, CO) and mouse anti-γH2AX (JBW103, Upstate, Charlottesville, VA) were allowed to bind for 2 h and immunocomplexes were detected using secondary anti-rabbit Alexa488- and anti-mouse Alexa564-conjugates, respectively (Molecular Probes, Invitrogen, Basel, Switzerland). Nuclei were stained with 4′,6-diamidino-2-phenylindole. Membranes were cut, mounted in MOWIOL and dried over night in the dark. Epifluorescence was analyzed using an Axiovert fluorescence microscope (Zeiss, Feldbach, Switzerland) and images were captured with fixed exposure times.

Single-cell electrophoresis (comet assays)

Single-cell electrophoresis was performed essentially as described with minor modifications (42). Briefly, cells were grown on 100 mm plates and subjected to the indicated treatments. After rinsing with PBS, cells were detached using a 0.005% trypsin solution, collected by centrifugation at 4°C with 250*g* and washed twice with ice-cold PBS. A total of 2.5×10^4 cells were resuspended in 10 μl PBS and added to 190 μl of 0.5% low-melting point agarose (Sigma) equilibrated to 37°C in a water bath. Remaining cells were immediately lysed with 1% sodium dodecyl sulfate, 50 mM Tris–HCl pH 6.8 and 10% glycerol for later immunoblot analyses. The agarose cell suspension was subsequently distributed on dried, agarose-precoated fully frosted slides, covered with a coverslip and allowed to solidify on a precooled aluminium plate. Slides were overlaid with a third layer of agarose and then subjected to precooled lysis solution (1% Triton X-100; 2.5 M NaCl; 100 mM ethylenediaminetetraacetic acid; 10 mM Tris–HCl pH 10.0) for 1 h at 4°C in the dark. Afterward, slides were equilibrated to alkaline electrophoresis buffer (300 mM NaOH; 1 mM ethylenediaminetetraacetic acid) for 20 min to allow for unwinding of the DNA. The agarose-embedded cells were then subjected to horizontal electrophoresis for 30 min (∼0.74 V/cm; 300 mA) with corresponding slides running side by side to ensure equal electrophoresis conditions. Slides were neutralized for 20 min in 100 mM Tris–HCl pH 7.5 and allowed to dry over night in the dark. Before analysis, dried slides were reconstituted in water and stained with a SYBR green solution (Invitrogen) for 10 min. DNA migration was visualized by fluorescence microscopy and images were captured using a fluorescence microscope. For quantitative comparison, the tail moment (%DNA in tail multiplied by tail length) was calculated from >150 cells per condition by two individuals, blinded to the treatment groups, using the CometScore software package (TriTek, Sumerduck, VA). The linear range of the assay was determined by plotting the averaged scores (mean ± SEM) of both quantifications. Slopes and intercepts for regression lines were compared using the Graphpad Prism software package (GraphPad Software, San Diego, CA).

Cell cycle analyses

MEFs were treated with 1 μM etoposide for 1 h before the medium was replaced and the cells were cultured for an additional period of up to 48 h. At the indicated time points, cell samples were washed and trypsinized. Detached cells were fixed with precooled 70% ethanol at −30°C and the DNA was stained with propidium iodide. FACS analysis was performed using a FACScan (Beckman-Coulter) and a single-cell population of 25 000 cells was monitored for DNA content. Percentages of cells in G_1, S phase and G_2/M were estimated using WinMDI 2.9 freeware.

Protein extractions and immunoblot analyses

Cells were washed twice and scraped into ice-cold PBS. For detection of DNA-PKcs, pATM, pCHK1, pCHK2, nuclei were extracted with a high-salt extraction buffer containing 0.1% NP-40 essentially as described before (41). Protein concentrations were determined by the Bradford method. Alternatively, total cell lysates were prepared to analyze γH2AX levels. Therefore, cells were collected in ice-cold PBS, lysed with 1% sodium dodecyl sulfate, 50 mM Tris–HCl pH 6.8 and 10% glycerol, followed by sonification and boiling for 5 min. Protein concentrations were determined using the detergent-insensitive BCA assay (Pierce, Perbio Science, Lausanne, Switzerland). Protein (50–80 μg) was separated by sodium dodecyl sulfate–polyacrylamide gel electrophoresis, electro-transferred onto polyvinylidene difluoride membranes and probed with antibodies derived against DNA-PKcs (Ab-4 cocktail, Labvision, Fremont, CA), pATM (10H11.E12, Cell Signaling, Danvers, MA), pCHK1 (133D3, Cell Signaling), pCHK2 (Cell Signaling), γH2AX (Upstate), HIF-1α (mAb67 and NB100-479, Novus Biological), Ku70 (N3H10, Abcam, Cambridge, UK), Ku80 (QED Bioscience, San Diego, CA) and β-actin (Sigma). Bound antibodies were detected by respective secondary antibodies (Pierce) and visualized with ECL substrate (Pierce).

Messenger RNA quantification

Total RNA was extracted as described previously (41). Following reverse transcription (RT) of 5 μg total RNA, messenger RNA (mRNA) levels were quantified with 1% of the diluted complementary DNA reaction mix by quantitative polymerase chain reaction (qPCR) using a SybrGreen qPCR reagent kit (Sigma) in combination with a MX3000P light cycler (Stratagene, La Jolla, CA). Initial template concentrations of each sample were calculated by comparison with serial dilutions of a calibrated standard. To control for equal input levels, ribosomal protein S12 mRNA was determined and data expressed as ratios relative to S12 levels. Melting point analyses of amplified PCR products were performed after each run to verify specific amplification.

Transient transfections and reporter gene assays

MEF cells were transfected using polyethyleneimine as described previously (41). In brief, 2 μg reporter plasmid was cotransfected with 100 ng of pRL-CMV (Promega, Madison, WI). After 24 h, the cells were equally distributed onto 12-well plates and exposed to 20 or 0.2% oxygen for another 20 h. After cell lysis with passive lysis buffer (Promega), dual luciferase activity was determined according to the manufacturer's instructions (Promega). To generate the pGL3-mPrkdc luciferase reporter gene construct, the 5′-region of *Prkdc*, the gene encoding mouse DNA-PKcs, was amplified from genomic DNA derived from MEF cells, using specific *Nhe*I-flanked forward (5′-catcgctagcgcgcgacaaaagaaatctg-3′) and *Xho*I-flanked reverse (5′-tgcactcgagatcacgccggcaccgcttc-3′) PCR primers. The products were ligated into *Nhe*I and *Xho*I sites of pGL3basic (Promega). Sequencing confirmed that they were identical to the respective database entry (GenBank accession NT_039624), regardless of whether the genomic DNA was isolated from MEF-*Hif1a*$^{+/+}$*r*T or MEF-*Hif1a*$^{-/-}$*r*T. The pH3SVL hypoxia-inducible reporter gene has been described previously (43).

RNA interference

MEF cells were plated at a density of 2×10^6 cells per 150 mm culture plate and allowed to adhere over night. Cells were then transfected with 500 pmol of stealth RNA interference duplexes targeting either DNA-PKcs (5′-gagcaguauucagaggagaccuuaa-3′), Ku80 (5′-ccuaaaugacgaugaugaaacugaa-3′) or a control small interfering RNA (siRNA) (5′-gcuccggagaacuaccagaguauua-3′) using Lipofectamine 2000 according to the manufacturer's protocol (Invitrogen). The following day, cells were split and processed as described for immunoblot analyses or clonogenic assay.

Results

Etoposide induces cell cycle arrest in MEFs irrespective of the presence of HIF-1α

We had shown previously that chemosensitivity and radiosensitivity are increased in HIF-1α-deficient MEFs (29). To investigate the underlying mechanisms, colony formation, cell cycle distribution and p53 function were analyzed. As shown in Figure 1a, treatment with increasing doses of etoposide reduced colony formation more efficiently in HIF-1α-deficient MEFs than in wild-type MEFs, confirming our previous half maximal inhibitory concentration determinations using 3-(4,5-dimethylthiazol-2-yl)-2,5-diphenyl tetrazolium bromide assays (29).

Because corrupted cell cycle control could explain the enhanced susceptibility to etoposide in HIF-1α-deficient MEFs, we next assessed their ability to initiate cell cycle arrest in response to DNA damage. Therefore, the cells were treated with 1 μM etoposide for 1 h and subsequently cultured for up to 12 h. As shown in Figure 1b, 6 h after exposure to etoposide, the percentage of cells with a duplicated genome (4N) was equally increased in both cell lines, suggesting accumulation at the G_2/M checkpoint. Of interest, 12 h after etoposide administration, the fraction of cells in G_2/M was almost restored to the initial values and a substantial increase of cells in G_1 phase was denoted at this time point in both cell lines, providing evidence for re-entry from the G_2/M checkpoint into the cell cycle (Figure 1b). No further fluctuations were observed at later time points and neither the generation time nor the cell cycle distribution differed between untreated MEF-*Hif1a*$^{+/+}$*r*T and MEF-*Hif1a*$^{-/-}$*r*T (data not shown).

Since the MEF cell lines used in this work were originally immortalized by stable expression of SV40 large T antigen and

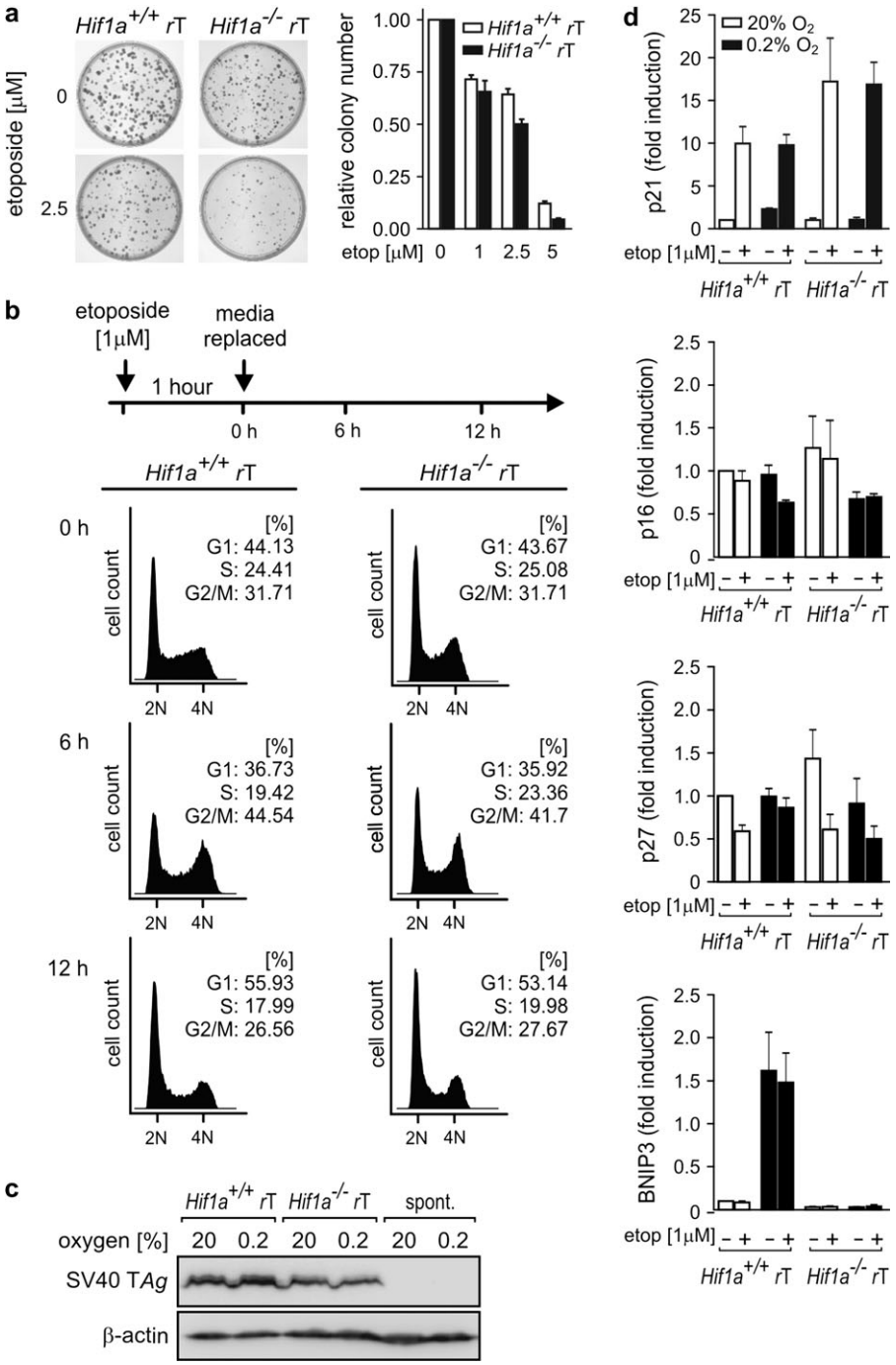

Fig. 1. Etoposide-induced cell cycle arrest in wild-type- and HIF-1α-deficient MEFs. (**a**) MEF-*Hif1a*$^{+/+}$*r*T and MEF-*Hif1a*$^{-/-}$*r*T were treated with 1, 2.5 and 5 μM etoposide for 1 h, trypsinized and plated in triplicates for each concentration. Colonies were counted after 6 days and normalized to the untreated control plates. Shown are mean values + SEMs of a representative experiment performed in triplicates. (**b**) Cell cycle distribution of MEF-*Hif1a*$^{+/+}$*r*T and MEF-*Hif1a*$^{-/-}$*r*T was determined by FACS analysis following treatment with 1 μM etoposide as indicated. (**c**) MEF lysates were immunoblotted for SV40 large T antigen and β-actin. Spontaneously immortalized MEFs (spont.) served as negative controls. (**d**) MEFs were treated with 1 μM etoposide for 8 h at either 20 or 0.2% oxygen and p21, p16, p27 and BNIP3 mRNA levels were quantified by RT–qPCR. Values were normalized to the mRNA levels of the housekeeping ribosomal protein S12. Mean values ± SEMs of three independent experiments are shown.

oncogenically transformed by infection with a recombinant retrovirus expressing activated H-*ras* 61L (12), differential expression of these two genes might have caused differential chemosensitivity. However, as shown in Figure 1c, no difference in large T antigen protein levels could be observed between the two cell lines. Human H-*ras* mRNA was undetectable by RT–qPCR, suggesting genomic silencing of the stably integrated complementary DNA (data not shown).

Finally, we considered differential functional inactivation of p53 by the large T antigen that might confound the response to DNA damage. However, after 8 h of etoposide treatment, a robust induction of the p53 target gene p21^{CIP1} was detected in both MEF lines, irrespective of the presence of HIF-1α ($P > 0.05$ Student's *t*-test, $n = 3$ independent experiments) or the cell culture oxygenation (Figure 1d). The p53 target genes Bax and Noxa were similarly regulated (data not shown).

The mRNA levels of the two cell cycle regulatory proteins $p16^{INK4a}$ and $p27^{KIP1}$ showed no marked differences in the two cell lines, whereas induction of the known proapoptotic HIF target gene BNIP3 confirmed hypoxia- and HIF-1-dependent target gene activation (Figure 1d). Thus, these data show that there are no major differences in p53 inactivation in the two cell lines due to cell immortalization.

Increased accumulation of DNA DSBs in HIF-1α-deficient MEF cells following etoposide treatment

While etoposide might affect DNA integrity by several mechanisms, inhibition of topoisomerase II, leading to stalled replication forks, is thought to result in DNA DSB in transcriptionally active cells (44). Therefore, we applied alkaline single-cell electrophoresis to quantify the DNA damage in MEF cells in response to treatment with etoposide. As reflected by the extended migration of fragmented DNA in comet tails, both cell lines showed an increase in DNA damage that dose dependently correlated with the etoposide concentrations (Figure 2a). At least 150 comet tails per experiment were quantified and DNA migration was expressed as 'tail moment' (Figure 2b). Of note, DNA migration was higher in MEF-*Hif1a*$^{-/-}$*r*T than in MEF-*Hif1a*$^{+/+}$*r*T in etoposide-treated as well as in untreated cells, suggesting HIF-1α-dependent changes in DNA integrity.

To characterize the nature of this increased susceptibility to DNA damage, aliquots of cells from the same experiments were analyzed by immunoblotting for phosphorylated histone 2AX (γH2AX), an established and sensitive marker of DNA DSB. In line with the comet data, MEF-*Hif1a*$^{-/-}$*r*T also showed increased γH2AX (Figure 2c). We next determined nuclear foci formation of p53-binding protein 1 (53BP1) and γH2AX at sites of DNA DSB. Indeed, in response to doses of etoposide as low as 0.25 μM, increased overlapping immunofluorescence of 53BP1 and γH2AX was seen in MEF-*Hif1a*$^{-/-}$*r*T compared with MEF-*Hif1a*$^{+/+}$*r*T (Figure 2d). These data suggest increased numbers of basal and inducible DNA DSBs in HIF-1α-deficient MEFs.

Analysis of DNA DSB repair pathways in MEF-Hif1a$^{+/+}$*rT and MEF-Hif1a*$^{-/-}$*rT*

Two conserved major DNA DSB repair pathways have been implicated in response to DNA DSB damage: homologous recombination and non-homologous end joining. When DNA DSBs accumulate, ataxia telangiectasia mutated/ataxia telangiectasia and Rad3 related (ATM/ATR) and DNA-PKcs kinases are activated by phosphorylation. Each of these kinases preferentially phosphorylates specific targets, leading to cell cycle arrest by phosphorylation of checkpoint kinases (CHK1 and CHK2) and/or sustained recruitment of DNA repair proteins to the DNA DSB foci via phosphorylation of H2AX. Upon treatment with etoposide, ATM Ser1981 autophosphorylation was strongly enhanced in both cell lines with a slightly higher degree in HIF-1α-deficient MEFs (Figure 3a). However, while basal CHK1 Ser345 phosphorylation was moderately increased in MEF-*Hif1a*$^{-/-}$*r*T, Thr387 autophosphorylation of CHK2, a downstream event of ATM activation, showed similar signals in the two cell lines (Figure 3a).

To identify the factors involved in dysregulated DNA DSB repair in HIF-1α-deficient MEF cells, candidate genes were screened by RT–qPCR of RNA derived from MEFs kept under normoxic (20% O_2) or hypoxic (0.2% O_2) conditions. Transcript levels of prolyl-4-hydroxylase domain (PHD3) and carbonic anhydrase IX were determined to control for hypoxia- and HIF-dependent gene expression (41), whereas growth arrest and DNA damage (GADD)153 mRNA was used as an HIF-independent hypoxia-inducible gene (45). As shown in Figure 3b, mRNA levels of 17 genes involved in DNA repair were measured. While none of these genes were induced by hypoxia, the mRNA levels of the three DNA-dependent protein kinase (DNA-PK) members, DNA-PKcs, Ku80 and Ku70, decreased with ongoing hypoxia, independently of HIF (Figure 3c). Interestingly, both basal and hypoxia-repressed mRNA levels of all three DNA-PK subunits were up to 3-fold reduced in MEF-*Hif1a*$^{-/-}$*r*T cells compared with MEF-*Hif1a*$^{+/+}$*r*T in this initial screening experiment (Figure 3c).

Dysregulation of DNA-PK complex members in HIF-1α-deficient MEF cells

Because the previously reported HIF-dependent chemoresistance was oxygenation independent, too (29), we further evaluated the HIF-1α-dependent differences in basal DNA-PK expression. As shown in Figure 4a, DNA-PKcs mRNA levels were significantly reduced in MEF-*Hif1a*$^{-/-}$*r*T when compared with MEF-*Hif1a*$^{+/+}$*r*T cells ($P < 0.05$; one sample *t*-test, $n = 3$ independent experiments performed in triplicates), irrespective of the oxygen concentration. Ku80 mRNA was also downregulated in MEF-*Hif1a*$^{-/-}$*r*T but the difference did not reach the level of significance. In contrast, Ku70, ATM and ATR mRNA levels were not affected by the absence of HIF-1α. HIF-dependent and/or oxygen-dependent gene regulation was controlled in the same samples by monitoring BNIP3 and GADD153 mRNA levels, respectively. As shown in Figure 4b, also the protein levels of all three DNA-PK subunits, including Ku70, were strikingly reduced in MEF-*Hif1a*$^{-/-}$*r*T cells.

The minichromosome maintenance-deficient 4 homolog (*Mcm4*) gene is structurally organized in a head-to-head arrangement with the *Prkdc* gene, encoding DNA-PKcs, only separated by a conserved CpG-rich promoter region of ~700 and 500 bp in humans and mice, respectively (46,47). Interestingly, MCM4 mRNA is regulated in a similar HIF-1α-dependent but oxygen-independent manner as DNA-PKcs (Figure 4a), suggesting transcriptional coregulation. To determine promoter activity, the shared 5′ region of the mouse *Prkdc* and *Mcm4* genes (a 695 bp DNA fragment spanning 16 bp 5′ of the *Mcm4* and 2 bp 3′ of the *Prkdc* translational start sites) was amplified by PCR using genomic DNA derived from MEF-*Hif1a*$^{+/+}$*r*T and MEF-*Hif1a*$^{-/-}$*r*T cells. Of note, no sequence variations between the two cell lines were observed in this region. Transient transfections of a luciferase reporter gene driven by this promoter region revealed a substantial decrease in reporter gene activity in MEF-*Hif1a*$^{-/-}$*r*T when compared with MEF-*Hif1a*$^{+/+}$*r*T cells (Figure 4c). Exposure of the transfected cells to 0.2% oxygen for 20 h reduced reporter gene activity by ~50%, irrespective of the presence of HIF-1α. Parallel transfections of the two cell lines with the hypoxia response element (HRE)-driven pH3SVL confirmed HIF-dependent hypoxic gene induction (Figure 4c). Forced expression of exogenous HIF-1α in MEF-*Hif1a*$^{-/-}$*r*T failed to increase the activity of the cotransfected 695 bp *Prkdc* promoter region, although transfected HIF-1α protein was clearly detectable by immunoblotting of parallel cultures (data not shown). While reduced promoter activity is sufficient to explain the decreased DNA-PKcs basal mRNA levels in HIF-1α-deficient MEFs, these data suggest that increased HIF-1α levels do not further induce mouse *Prkdc* gene expression, as expected from the lack of hypoxic induction of DNA-PKcs mRNA in wild-type MEF cells.

Downregulation of DNA-PKcs reduces cell growth in MEF-Hif1a$^{+/+}$*rT*

To further test the impact of reduced DNA-PK protein levels on chemoresistance in our cellular model, Ku80 and DNA-PKcs were transiently downregulated by RNA interference in MEF-*Hif1a*$^{+/+}$*r*T. Protein levels of both subunits were efficiently reduced by siRNA transfection as confirmed by immunoblotting (Figure 5a). Depletion of Ku80 protein levels sensitized MEF-*Hif1a*$^{+/+}$*r*T to etoposide as assessed by quantification of γH2AX accumulation via immunoblotting (Figure 5b). Knockdown of DNA-PKcs was only effective at higher dose, marking Ku80 as a major factor in the etoposide-induced DNA damage response in MEFs. These observations are in line with previous reports on differential etoposide sensitivity in hamster cells deficient for Ku80, whereas murine DNA-PKcs mutant cell lines showed no hypersensitivity to etoposide (48).

To analyze etoposide sensitivity on the cellular levels, colony formation assays were performed (Figure 5c). Surprisingly, the total number of colonies remained unchanged in untreated MEF-*Hif1a*$^{+/+}$*r*T after downregulation of either Ku80 or DNA-PKcs (Figure 5d). Etoposide treatment slightly decreased the number of surviving cells, but colony number was again not further affected by Ku80 or DNA-PKcs siRNA (Figure 5d). While the colony number remained unaffected in untreated MEF-*Hif1a*$^{-/-}$*r*T, etoposide

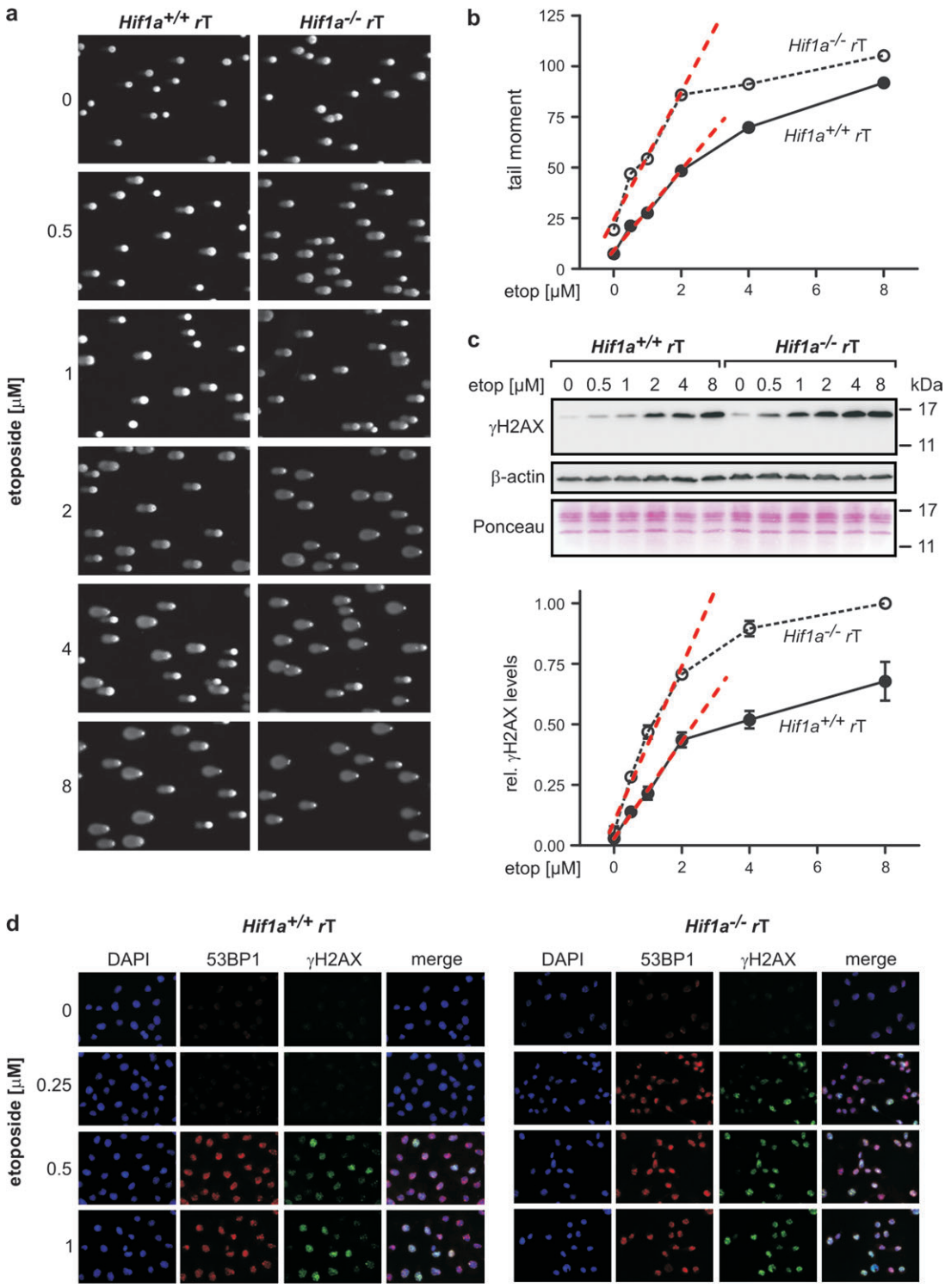

Fig. 2. DNA fragmentation in wild-type- and HIF-1α-deficient MEFs after a genotoxic insult. (**a**) DNA fragmentation in MEF-*Hif1a*$^{+/+}$*r*T and MEF-*Hif1a*$^{-/-}$*r*T cells was quantified by single-cell electrophoresis following exposure to increasing amounts of etoposide for 1 h. DNA was stained with SYBR green and all images were acquired with fixed exposure times. (**b**) DNA fragmentation was quantified by determining the tail moment of at least 150 comets per condition using CometScore software. Differences between the *y*-axis intercepts of regression lines (dashed red lines) within the linear range of the assay were highly significant ($P < 0.01$). (**c**) Aliquots of cell cultures from *A* were subjected to immunoblotting for γH2AX. Band intensities were quantified by densitometry and normalized to β-actin levels. As in (**b**), linear regression was performed for treatments with up to 2 μM etoposide (dashed red lines), revealing highly different slopes ($P < 0.0001$). Ponceau staining served to demonstrate equal extraction of histones. (**d**) MEF cells were grown on lumox membranes and treated with up to 1 μM etoposide for 1 h. Immunofluorescence was performed using antibodies directed against 53BP1 and γH2AX and nuclei were counterstained with 4′,6-diamidino-2-phenylindole (DAPI). All data are given as mean values ± SEMs.

treatment dramatically decreased colony formation in this cell line (Figure 5d), confirming the results shown in Figure 1a.

In contrast to the colony number, the total cell area of samples treated with siRNA targeting DNA-PKcs was decreased by ~50% in untreated and etoposide-treated MEF-*Hif1a*$^{+/+}$*r*T, whereas control siRNA or siRNA targeting Ku80 had no such effect (Figure 5e). Because the total cell area reflects cellular growth, these data suggest a specific role for the catalytic subunit

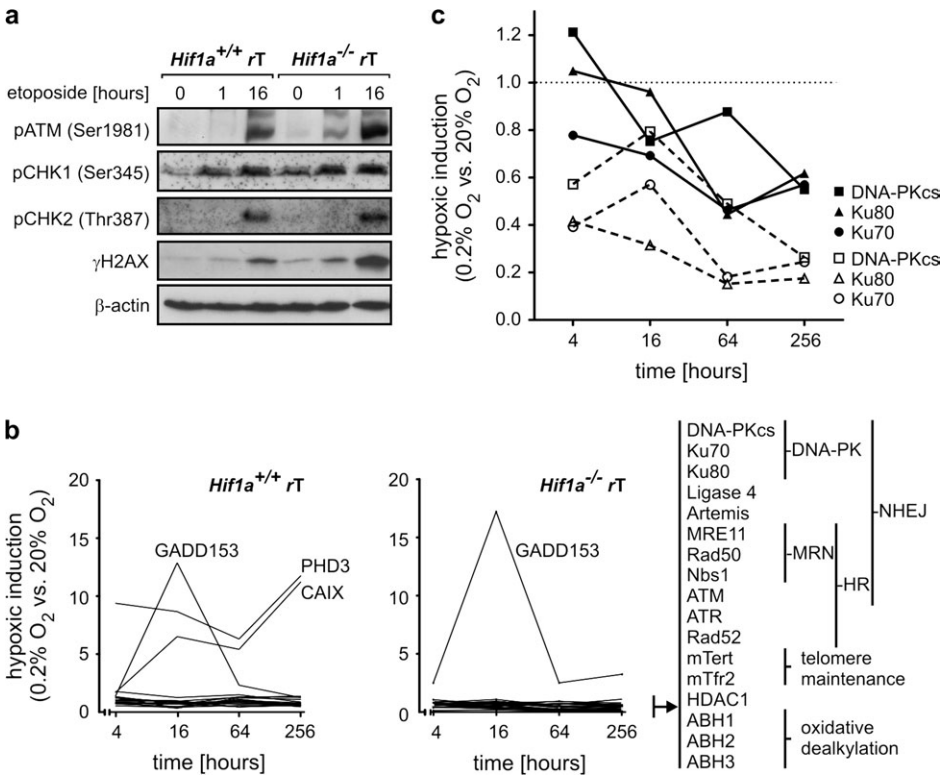

Fig. 3. Analysis of DNA repair pathways in wild-type- and HIF-1α-deficient MEFs. (**a**) MEF-*Hif1a*$^{+/+}$*r*T and MEF-*Hif1a*$^{-/-}$*r*T cells were treated with 1 μM etoposide for 0–16 h under normoxic conditions. Phosphorylation of ATM, CHK1, CHK2 and H2AX was analyzed by immunoblotting using phosphoprotein-specific antibodies. β-Actin served as loading control. (**b**) MEF-*Hif1a*$^{+/+}$*r*T and MEF-*Hif1a*$^{-/-}$*r*T cells were permanently cultured at 20 or 0.2% O_2 for 0, 4, 16, 64 or 256 h in a hypoxic workstation. Transcript levels of 17 candidate genes involved in DNA repair were quantified by RT–qPCR. Hypoxic induction factors are shown following normalization to the mRNA levels of ribosomal protein S12. (**c**) Hypoxic downregulation of DNA-PK complex members in MEF-*Hif1a*$^{+/+}$*r*T (filled symbols) and MEF-*Hif1a*$^{-/-}$*r*T (open symbols) as determined in (**b**).

of DNA-PK in cell proliferation, most probably due to sustaining genomic integrity.

Cell model-specific effects of HIF-dependent chemoresistance

To test our findings in an independent HIF-1α-deficient model, we generated HIF-1α mRNA knockdown cell lines by stable short hairpin RNA (shRNA) transfection in MEF-*Hif1a*$^{+/+}$*r*T cells. However, partial HIF-1α mRNA knockdown only marginally affected the expression of DNA-PK complex members (data not shown). Therefore, we repeated our experiments in an HIF-1α-deficient MEF cell line derived from an independent knockout mouse strain (40). These cell lines were named MEF-*Hif1a*$^{+/+}$T and MEF-*Hif1a*$^{-/-}$T since they were not transformed by H-*ras*. However, whereas MEF-*Hif1a*$^{-/-}$*r*T showed the expected increased susceptibility to etoposide, MEF-*Hif1a*$^{-/-}$T cells were equally sensitive to etoposide as the corresponding wild-type control (Figure 6a).

In line with this finding, no difference in mRNA and protein levels of DNA-PKcs could be detected between MEF-*Hif1a*$^{+/+}$T and MEF-*Hif1a*$^{-/-}$T, whereas DNA-PKcs was clearly lower in MEF-*Hif1a*$^{-/-}$*r*T than in MEF-*Hif1a*$^{+/+}$*r*T (Figure 6b, left panel, and data not shown). To control for the genotype of the MEF-*Hif1a*$^{-/-}$T cells, HIF-1α immunoblotting of nuclear extracts was included. Interestingly, following prolonged exposure, anti-HIF-1α antibodies reacted with a smaller but still hypoxia-inducible protein detectable in MEF-*Hif1a*$^{-/-}$T but not in MEF-*Hif1a*$^{-/-}$*r*T (Figure 6b, right panel). This supposedly truncated HIF-1α protein cannot be directly transcriptionally active since it is derived from a targeted deletion of exon 2, containing the basic helix-loop-helix DNA-binding region of HIF-1α. Indeed, protein levels of the HIF target gene PHD2 were no longer hypoxically induced in both HIF-1α-deficient cell lines (Figure 6b, right panel). Finally, the levels of SV40 large T antigen were similar in all four cell lines, ruling out major differences due to changes in large T levels. Another major difference between the two cell lines might be the H-*ras* levels. However, using RT–qPCR, we could not detect any H-*ras* mRNA, neither in the MEF-*Hif1a*$^{+/+}$T/MEF-*Hif1a*$^{-/-}$T nor in the MEF-*Hif1a*$^{+/+}$*r*T/MEF-*Hif1a*$^{-/-}$*r*T cell lines, whereas diluted H-*ras* plasmid complementary DNA was still detectable (data not shown).

To further confirm lack of HIF-dependent transcriptional activity, MEF-*Hif1a*$^{+/+}$T and MEF-*Hif1a*$^{-/-}$T cells were transiently transfected with the HRE-driven pH3SVL reporter plasmid. As expected, there was no residual hypoxic induction of HIF-dependent reporter gene expression in MEF-*Hif1a*$^{-/-}$T (Figure 6c). Similar results were obtained for the endogenous transcripts of BNIP3 that were only induced in HIF-1α-containing MEF-*Hif1a*$^{+/+}$T (Figure 6d). Induction of GADD153 in both cell lines confirmed their hypoxic status.

Discussion

Due to microenvironmental changes as well as oncogenic transformation, HIF-1α levels are constitutively increased in solid tumors. This work proposes a new molecular link between HIF-1α and tumor therapy resistance by demonstrating that both basal and etoposide-induced DNA damage is increased in an HIF-1α-deficient cell model. Transcript levels of DNA-PK complex members, DNA-PKcs and Ku80, were found to be downregulated in HIF-1α-deficient cells previously found to have a higher susceptibility to chemotherapeutics introducing DNA DSBs. On the protein level, not only DNA-PKcs and Ku80 but also the third DNA-PK member Ku70 was decreased in these HIF-deficient cells. The reduced Ku70 protein levels, despite similar mRNA levels, are probably explained by the lack of mutual protein stabilization of the three DNA-PK complex members: radiosensitive chinese hamster ovary cells expressing reduced levels of

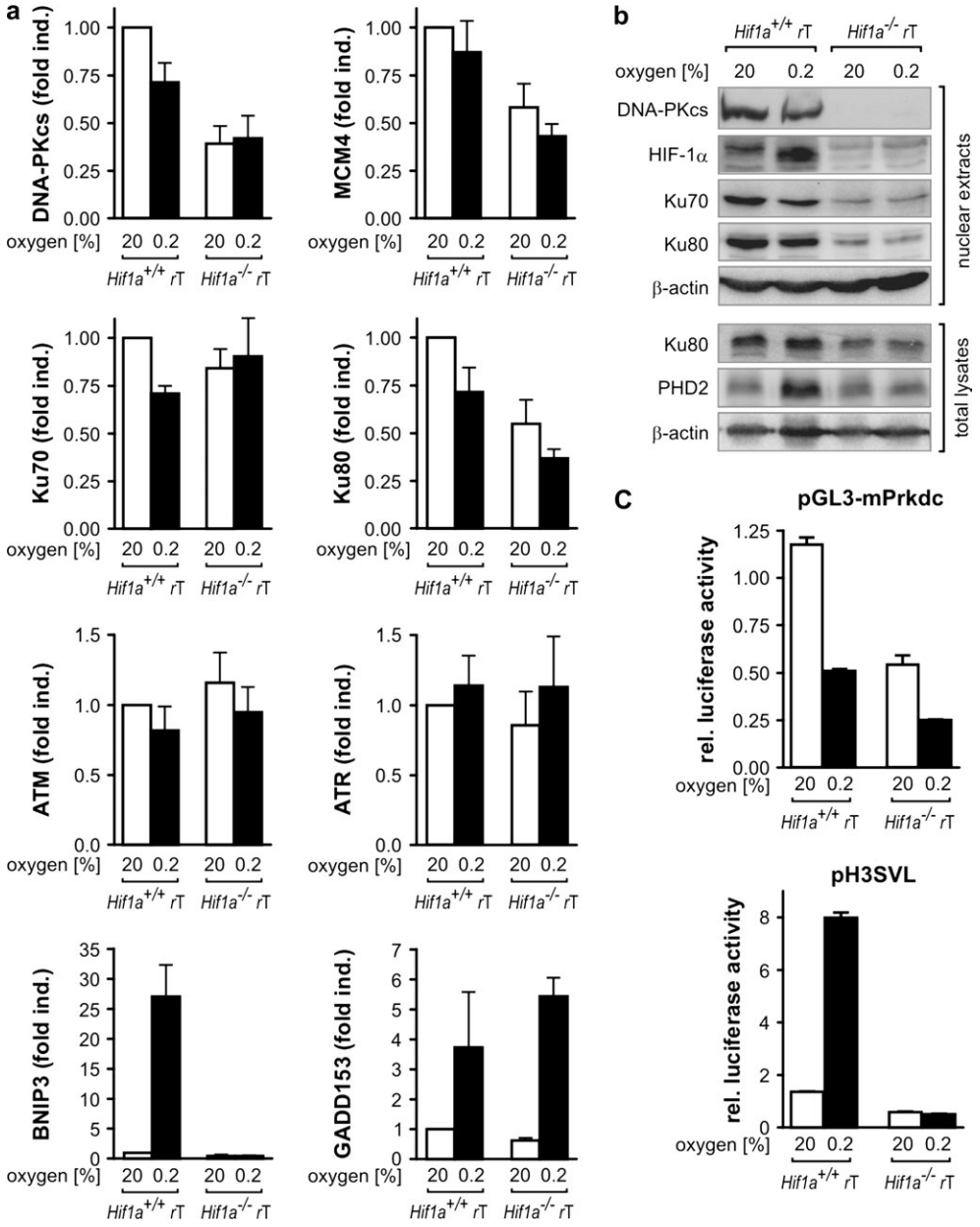

Fig. 4. Reduced expression of DNA-PK subunits in HIF-1α-deficient MEFs. (**a**) mRNA levels of the three DNA-PK subunits, DNA-PKcs, Ku70 and Ku80, as well as MCM4, ATM and ATR, were quantified in MEF-*Hif1a*$^{+/+}$*r*T and MEF-*Hif1a*$^{-/-}$*r*T cells after exposure to 0.2% oxygen for 16 h. BNIP3 and GADD153 mRNA levels were determined as controls. All values were normalized to ribosomal protein S12 mRNA levels. Mean induction factors + SEM of three independent experiments performed in triplicates are shown. (**b**) Immunoblot analyses of DNA-PKcs, Ku70 and Ku80 in nuclear extracts of MEF cells treated as above. HIF-1α protein levels were determined to control for hypoxic induction and genotype. β-Actin levels were determined as loading control. Reduced levels of Ku80 were confirmed in total cell lysates (bottom panel) and HIF-dependent hypoxic induction of PHD2 is shown. (**c**) Relative luciferase activities were determined in MEF cells transiently cotransfected with 2 μg pGL3-mPrkdc or pH3SVL and 0.1 μg pRL-CMV as transfection control. Transfected cultures were incubated for 20 h at either 20 or 0.2% oxygen and dual luciferase activity was measured. Data are shown as mean values of hexaplicates + SEM.

Ku80 also showed lowered levels of Ku70 and forced expression of Ku86 in such cells concomitantly restored Ku70 protein levels (49,50). Importantly, DNA-PK levels inversely correlate with tumor therapy efficiency (such as etoposide treatment) in a broad range of cell models, including human cancer cell lines (51–53). In line with these studies, downregulation of Ku80 increased the DNA damage response and downregulation of DNA-PKcs reduced cell growth in MEFs. Of note, transient removal of DNA-PKcs did not completely phenocopy the increase in chemosensitivity by loss of HIF-1α in MEF-*Hif1a*$^{-/-}$*r*T, suggesting that additional mechanisms contribute to the chemosensitivity in these cells.

Supporting our results using HIF-1β-deficient hepatoma cells, Um *et al.* (54) reported induction of DNA-PKcs, Ku70 and Ku80 by hypoxia and iron chelation in an HIF-1β-dependent manner. While Ku has been reported to be induced by hypoxia in other cell types as well (55,56), we could not observe any hypoxia-inducible Ku or DNA-PKcs expression in MEF cells. How could an HIF-dependent but non-hypoxia-inducible gene expression be explained? Genetically, HIF-1α-deficient cells are well known to have even lower HIF target gene levels than wild-type cells when both cell lines are cultured under the standard 'oxic' 20% oxygen conditions (57). As HIF-1α protein accumulation under hypoxic condition reaches strikingly

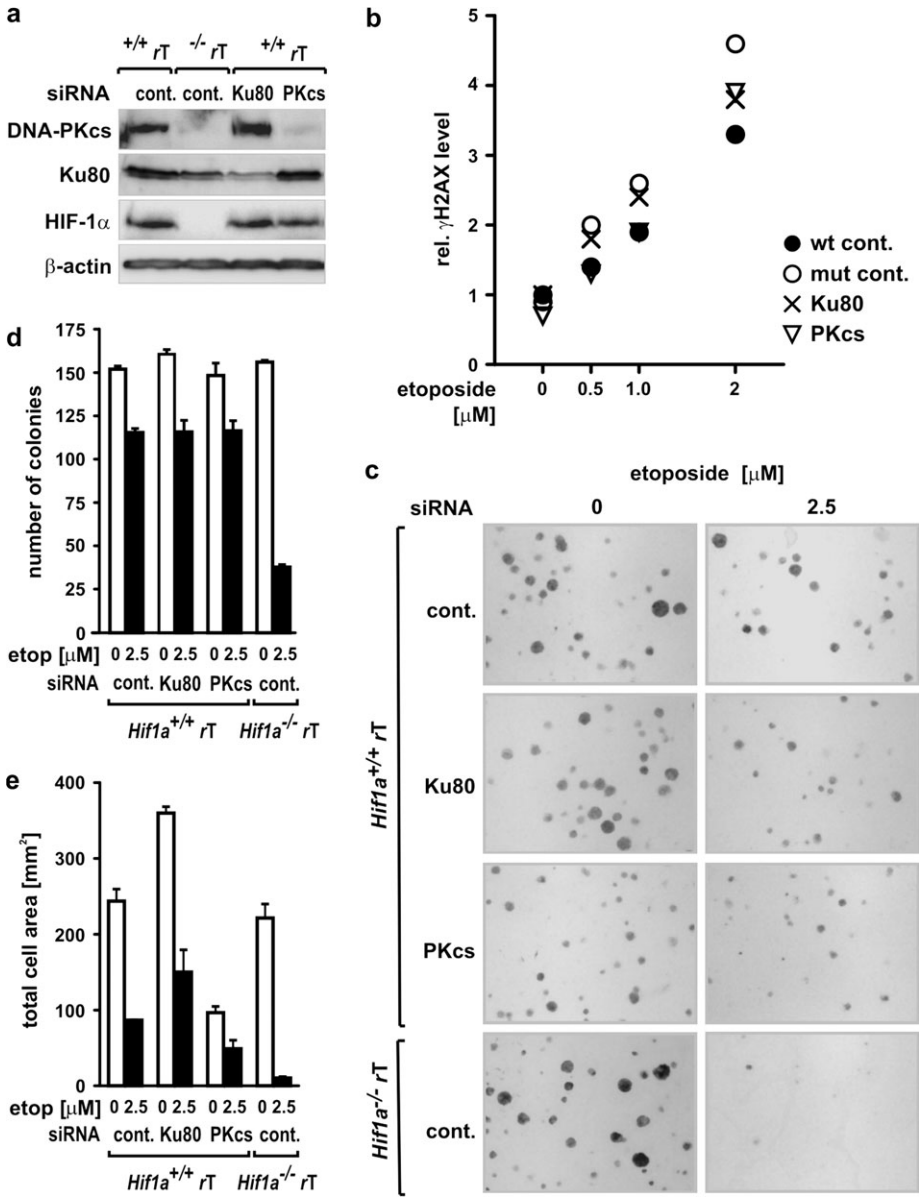

Fig. 5. Downregulation of Ku80 augments H2AX phosphorylation in etoposide-treated MEF-*Hif1a*$^{+/+}$*r*T. (**a**) The efficiency of siRNA-mediated downregulation of DNA-PKcs and Ku80 in MEF-*Hif1a*$^{+/+}$*r*T cells was determined by immunoblotting of nuclear extracts. Normoxic HIF-1α and β-actin were included as cell line and loading controls, respectively. (**b**) siRNA-mediated downregulation of Ku80 or DNA-PKcs in MEF-*Hif1a*$^{+/+}$*r*T cells (wt) followed by determination of their etoposide sensitivity. The cells were treated with the indicated etoposide concentrations for 1 h and γH2AX levels were quantified by immunoblotting and light imaging. Data were normalized to untreated MEF-*Hif1a*$^{+/+}$*r*T. For comparison, MEF-*Hif1a*$^{-/-}$*r*T cells (mut) were included. An independent repetition revealed similar results. (**c**) MEF-*Hif1a*$^{+/+}$*r*T cells were treated as in (**b**) followed by colony formation assays. Crystal violet stained colonies were depicted using identical magnification and representative sections are shown. Note the highly variable colony sizes specifically seen in MEF-*Hif1a*$^{+/+}$*r*T treated with siRNA directed against DNA-PKcs and MEF-*Hif1a*$^{-/-}$*r*T treated with control siRNA. (**d**) Number of colonies formed per 100 mm plate. (**e**) Total cell area per 100 mm plate as determined by computer-assisted analysis using ImageJ software. All data are given as mean of triplicates + SEM.

high levels, normoxic HIF-1α protein expression usually escapes the detection limit of standard methods in subconfluent cells cultured at 20% oxygen. However, longer exposures of immunoblots revealed that HIF-1α protein indeed is also present in normoxic cells. The concept of 'oxic' HIF-1α was further developed by Giaccia *et al.* who showed that loss of HIF-1α under aerobic conditions accelerated cellular senescence in a macrophage migration inhibitory factor-dependent manner (58). The *VE-cadherin* gene has been reported to be induced by HIF-2 but not by hypoxia (59). Finally, Zeng *et al.* (60) recently reported that HIF-1α decreased the sensitivity of lung cancer cells to paclitaxel under normoxic conditions, further supporting our data. Thus, these examples demonstrate that the low concentrations of HIF-1α under normoxic conditions are sufficient for certain cellular processes. Translated to tumor biology, this could imply that slight changes in HIF-1α mRNA expression levels by oncogenic transformation and inflammatory processes early in tumor formation might already lead to changes in HIF target gene expression, even before the growing tumor creates severely hypoxic regions with massively induced HIF-1α protein.

Interestingly, an independent HIF-1α-deficient MEF cell line derived from another knockout mouse model, supposedly containing low levels of a truncated version of HIF-1α, neither showed increased chemosensitivity nor reduced DNA-PKcs protein levels (Figure 6). Thus, one may conclude that only the complete absence of HIF-1α in MEF cells conferred oxic chemosensitivity and residual HIF-1α might be sufficient to reverse this effect. In line with this hypothesis, partial downregulation of HIF-1α by shRNA interference only marginally

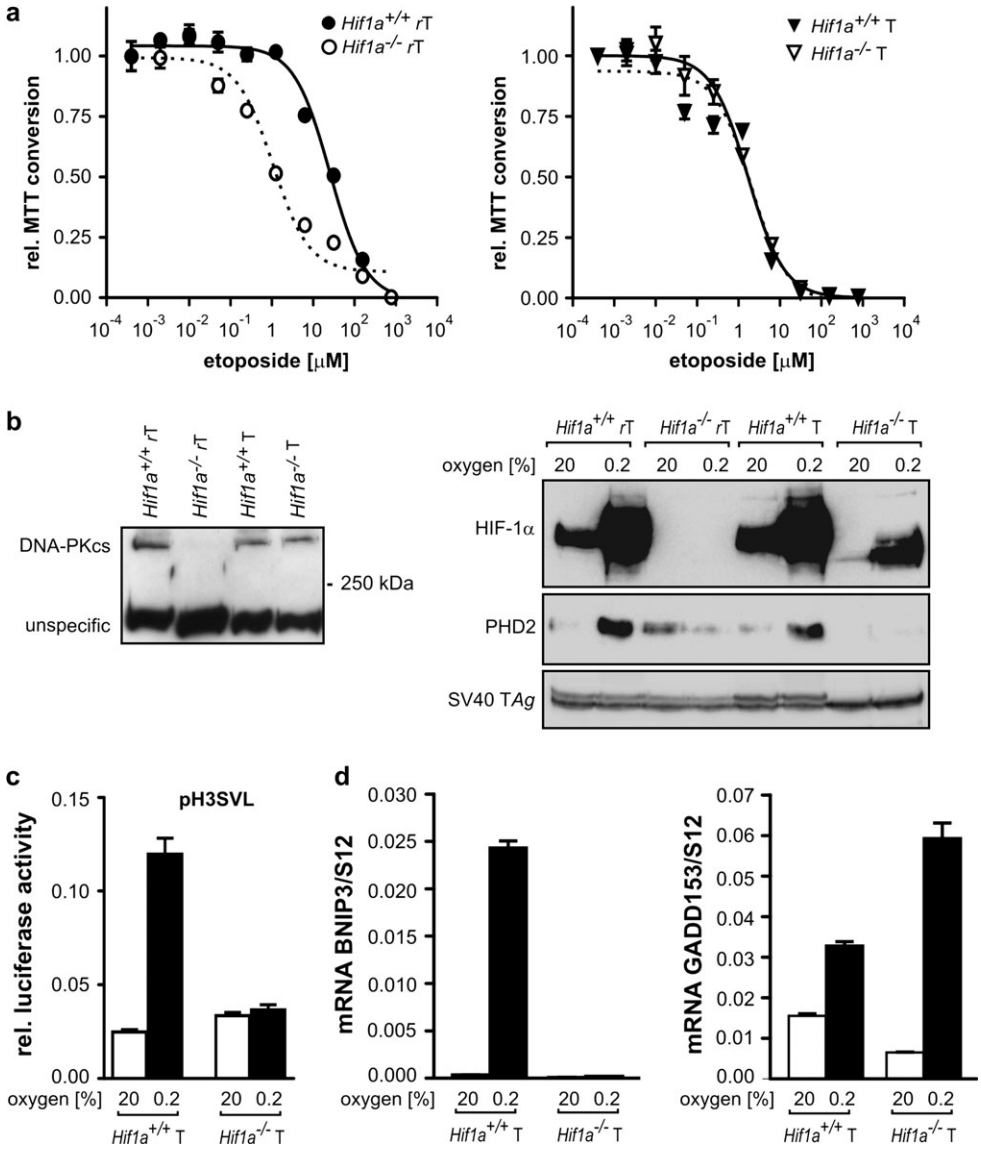

Fig. 6. Increased chemosensitivity to etoposide is not observed in HIF-1α knockout MEFs containing residual truncated HIF-1α. (**a**) Relative 3-(4,5-dimethylthiazol-2-yl)-2,5-diphenyl tetrazolium bromide (MTT) conversion in response to etoposide treatment for 24 h was determined in two independent MEF cell lines distinguished by the presence (*r*T) or absence (T) of H-*ras* transfection. Cultures were treated in triplicates and values normalized to untreated control cells. Data are given as mean values of triplicates + SEM. (**b**) Nuclear protein was subjected to immunoblot analysis of DNA-PKcs (left) or HIF-1α, PHD2 and SV40 large T antigen protein levels. (**c**) MEF-*Hif1a*$^{+/+}$T and MEF-*Hif1a*$^{-/-}$T were transiently cotransfected with 2 μg pH3SVL and 0.1 μg pRL-CMV as transfection control. Dual luciferase activity was measured and values expressed as mean of hexaplicates + SEM. (**d**) BNIP3 and GADD153 mRNA levels were quantified by RT–qPCR in MEF-*Hif1a*$^{+/+}$T and MEF-*Hif1a*$^{-/-}$T after exposure to 0.2% oxygen for 16 h. All values were normalized to ribosomal protein S12 mRNA levels and are shown as mean + SEM of experiments performed in triplicates.

affected chemoresistance in MEF-*Hif1a*$^{+/+}$*r*T cells, whereas hypoxic induction of HIF-1α target genes was strongly impaired (data not shown). DNA-binding activity appears not to be required, ruling out a direct transcriptional function. Indeed, despite the presence of putative HRE sites, the DNA-PKcs promoter was not found to be induced by hypoxia. Rather, the DNA-PKcs promoter as well as endogenous DNA-PKcs mRNA expression were downregulated by the (complete) absence of HIF-1α. A recent report has described a non-transcriptional role for c-myc in the control of DNA replication, giving precedence to alternative functions of transcription factors (61). Thus, it will be an intriguing question for future research to elucidate whether HIF-1α has similar non-transcriptional functions, e.g. by assembling other subunits into large protein complexes.

In apparent contrast to our findings, Huang *et al.* (62) reported that HIF is responsible for genomic instability by downregulating several factors involved in DNA repair. However, only treatments that cause DNA DSBs were effectively impaired by HIF in our model system (29). While DNA DSB repair by non-homologous end joining confers resistance to DNA DSB-causing agents, non-homologous end joining is an error-prone process. Thus, HIF-dependent DNA DSB repair might even boost genomic instability and hence malignant progression.

Funding

The 6th Framework Programme of the European Commission (EUROXY LSHC-CT-2003-502932/SBF 03.0647-2 to R.H.W.); Krebsliga des Kantons Zürich to R.H.W.; Kurt und Senta Herrmann-Stiftung to S.W. and R.H.W.; Sassella Stiftung to D.P.S.;

Forschungskredit of the University of Zürich to D.P.S.; and Swiss National Science Foundation (SNF 3100AO-116047/1 to R.H.W.).

Acknowledgements

The authors wish to thank R.S.Johnson and G.L.Semenza for the gift of cell lines, P.Spielmann for excellent technical assistance and G.Camenisch for helpful advice.

Conflict of Interest Statement: None declared.

References

1. Brown,J.M. *et al*. (1998) The unique physiology of solid tumors: opportunities (and problems) for cancer therapy. *Cancer Res.*, **58**, 1408–1416.
2. Brown,J.M. *et al*. (2004) Exploiting tumour hypoxia in cancer treatment. *Nat. Rev. Cancer*, **4**, 437–447.
3. Pouysségur,J. *et al*. (2006) Hypoxia signalling in cancer and approaches to enforce tumour regression. *Nature*, **441**, 437–443.
4. Wenger,R.H. (2002) Cellular adaptation to hypoxia: O_2-sensing protein hydroxylases, hypoxia-inducible transcription factors, and O_2-regulated gene expression. *FASEB J.*, **16**, 1151–1162.
5. Schofield,C.J. *et al*. (2004) Oxygen sensing by HIF hydroxylases. *Nat. Rev. Mol. Cell Biol.*, **5**, 343–354.
6. Wenger,R.H. *et al*. (2005) Integration of oxygen signaling at the consensus HRE. *Sci. STKE*, **2005**, re12.
7. Seagroves,T.N. *et al*. (2001) Transcription factor HIF-1 is a necessary mediator of the Pasteur effect in mammalian cells. *Mol. Cell. Biol.*, **21**, 3436–3444.
8. Svastova,E. *et al*. (2004) Hypoxia activates the capacity of tumor-associated carbonic anhydrase IX to acidify extracellular pH. *FEBS Lett.*, **577**, 439–445.
9. Minchenko,A. *et al*. (2002) Hypoxia-inducible factor-1 (HIF-1) mediated expression of the 6-phosphofructo-2-kinase/fructose-2,6-bisphosphatase-3 (*PFKBF3*) gene: its possible role in the Warburg effect. *J. Biol. Chem.*, **277**, 6183–6187.
10. Schroeder,T. *et al*. (2005) Spatial heterogeneity and oxygen dependence of glucose consumption in R3230Ac and fibrosarcomas of the Fischer 344 rat. *Cancer Res.*, **65**, 5163–5171.
11. Ryan,H.E. *et al*. (1998) HIF-1α is required for solid tumor formation and embryonic vascularization. *EMBO J.*, **17**, 3005–3015.
12. Ryan,H.E. *et al*. (2000) Hypoxia-inducible factor-1α is a positive factor in solid tumor growth. *Cancer Res.*, **60**, 4010–4015.
13. Krieg,M. *et al*. (2000) Up-regulation of hypoxia-inducible factors HIF-1α and HIF-2α under normoxic conditions in renal carcinoma cells by von Hippel-Lindau tumor suppressor gene loss of function. *Oncogene*, **19**, 5435–5443.
14. Zundel,W. *et al*. (2000) Loss of PTEN facilitates HIF-1-mediated gene expression. *Genes Dev.*, **14**, 391–396.
15. Ravi,R. *et al*. (2000) Regulation of tumor angiogenesis by p53-induced degradation of hypoxia-inducible factor 1α. *Genes Dev.*, **14**, 34–44.
16. Jiang,B.H. *et al*. (1997) V-SRC induces expression of hypoxia-inducible factor 1 (HIF-1) and transcription of genes encoding vascular endothelial growth factor and enolase 1: involvement of HIF-1 in tumor progression. *Cancer Res.*, **57**, 5328–5335.
17. Zhong,H. *et al*. (1999) Overexpression of hypoxia-inducible factor 1α in common human cancers and their metastases. *Cancer Res.*, **59**, 5830–5835.
18. Birner,P. *et al*. (2000) Overexpression of hypoxia-inducible factor 1α is a marker for an unfavorable prognosis in early-stage invasive cervical cancer. *Cancer Res.*, **60**, 4693–4696.
19. Aebersold,D.M. *et al*. (2001) Expression of hypoxia-inducible factor-1α: a novel predictive and prognostic parameter in the radiotherapy of oropharyngeal cancer. *Cancer Res.*, **61**, 2911–2916.
20. Koukourakis,M.I. *et al*. (2002) Hypoxia-inducible factor (HIF1A and HIF2A), angiogenesis, and chemoradiotherapy outcome of squamous cell head-and-neck cancer. *Int. J. Radiat. Oncol. Biol. Phys.*, **53**, 1192–1202.
21. Bachtiary,B. *et al*. (2003) Overexpression of hypoxia-inducible factor 1α indicates diminished response to radiotherapy and unfavorable prognosis in patients receiving radical radiotherapy for cervical cancer. *Clin. Cancer Res.*, **9**, 2234–2240.
22. Generali,D. *et al*. (2006) Hypoxia-inducible factor-1α expression predicts a poor response to primary chemoendocrine therapy and disease-free survival in primary human breast cancer. *Clin. Cancer Res.*, **12**, 4562–4568.
23. Comerford,K.M. *et al*. (2002) Hypoxia-inducible factor-1-dependent regulation of the multidrug resistance (MDR1) gene. *Cancer Res.*, **62**, 3387–3394.
24. Wartenberg,M. *et al*. (2003) Regulation of the multidrug resistance transporter P-glycoprotein in multicellular tumor spheroids by hypoxia-inducible factor (HIF-1) and reactive oxygen species. *FASEB J.*, **17**, 503–505.
25. Erler,J.T. *et al*. (2004) Hypoxia-mediated down-regulation of Bid and Bax in tumors occurs via hypoxia-inducible factor 1-dependent and -independent mechanisms and contributes to drug resistance. *Mol. Cell. Biol.*, **24**, 2875–2889.
26. Sermeus,A. *et al*. (2008) Hypoxia induces protection against etoposide-induced apoptosis: molecular profiling of changes in gene expression and transcription factor activity. *Mol. Cancer*, **7**, 27.
27. Wenger,R.H. *et al*. (1998) Up-regulation of hypoxia-inducible factor-1α is not sufficient for hypoxic/anoxic p53 induction. *Cancer Res.*, **58**, 5678–5680.
28. Moeller,B.J. *et al*. (2006) HIF-1 and tumour radiosensitivity. *Br. J. Cancer*, **95**, 1–5.
29. Unruh,A. *et al*. (2003) The hypoxia-inducible factor-1α is a negative factor for tumor therapy. *Oncogene*, **22**, 3213–3220.
30. Zhang,X. *et al*. (2004) Enhancement of hypoxia-induced tumor cell death *in vitro* and radiation therapy *in vivo* by use of small interfering RNA targeted to hypoxia-inducible factor-1α. *Cancer Res.*, **64**, 8139–8142.
31. Williams,K.J. *et al*. (2005) Enhanced response to radiotherapy in tumours deficient in the function of hypoxia-inducible factor-1. *Radiother. Oncol.*, **75**, 89–98.
32. Moeller,B.J. *et al*. (2005) Pleiotropic effects of HIF-1 blockade on tumor radiosensitivity. *Cancer Cell*, **8**, 99–110.
33. Brown,L.M. *et al*. (2006) Reversing hypoxic cell chemoresistance *in vitro* using genetic and small molecule approaches targeting hypoxia inducible factor-1. *Mol. Pharmacol.*, **69**, 411–418.
34. Song,X. *et al*. (2006) Hypoxia-induced resistance to cisplatin and doxorubicin in non-small cell lung cancer is inhibited by silencing of HIF-1α gene. *Cancer Chemother. Pharmacol.*, **58**, 108–111.
35. Li,J. *et al*. (2006) Knockdown of hypoxia-inducible factor-1α in breast carcinoma MCF-7 cells results in reduced tumor growth and increased sensitivity to methotrexate. *Biochem. Biophys. Res. Commun.*, **342**, 1341–1351.
36. Sasabe,E. *et al*. (2007) The involvement of hypoxia-inducible factor-1α in the susceptibility to gamma-rays and chemotherapeutic drugs of oral squamous cell carcinoma cells. *Int. J. Cancer*, **120**, 268–277.
37. Li,L. *et al*. (2006) Hypoxia-inducible factor-1 inhibition in combination with temozolomide treatment exhibits robust antitumor efficacy *in vivo*. *Clin. Cancer Res.*, **12**, 4747–4754.
38. Martinive,P. *et al*. (2006) Preconditioning of the tumor vasculature and tumor cells by intermittent hypoxia: implications for anticancer therapies. *Cancer Res.*, **66**, 11736–11744.
39. Ji,Z. *et al*. (2006) Induction of hypoxia-inducible factor-1α overexpression by cobalt chloride enhances cellular resistance to photodynamic therapy. *Cancer Lett.*, **244**, 182–189.
40. Feldser,D. *et al*. (1999) Reciprocal positive regulation of hypoxia-inducible factor 1α and insulin-like growth factor 2. *Cancer Res.*, **59**, 3915–3918.
41. Stiehl,D.P. *et al*. (2006) Increased prolyl 4-hydroxylase domain proteins compensate for decreased oxygen levels. Evidence for an autoregulatory oxygen-sensing system. *J. Biol. Chem.*, **281**, 23482–23491.
42. Singh,N.P. *et al*. (1988) A simple technique for quantitation of low levels of DNA damage in individual cells. *Exp. Cell Res.*, **175**, 184–191.
43. Wanner,R.M. *et al*. (2000) Epolones induce erythropoietin expression via hypoxia-inducible factor-1α activation. *Blood*, **96**, 1558–1565.
44. Burden,D.A. *et al*. (1998) Mechanism of action of eukaryotic topoisomerase II and drugs targeted to the enzyme. *Biochim. Biophys. Acta*, **1400**, 139–154.
45. Carrière,A. *et al*. (2004) Mitochondrial reactive oxygen species control the transcription factor CHOP-10/GADD153 and adipocyte differentiation: a mechanism for hypoxia-dependent effect. *J. Biol. Chem.*, **279**, 40462–40469.
46. Connelly,M.A. *et al*. (1998) The promoters for human DNA-PKcs (PRKDC) and MCM4: divergently transcribed genes located at chromosome 8 band q11. *Genomics*, **47**, 71–83.
47. Saito,T. *et al*. (1998) Mouse cdc21 only 0.5 kb upstream from DNA-PKcs in a head-to-head organization: an implication of co-evolution of ATM family members and cell cycle regulating genes. *Mamm. Genome*, **9**, 769–772.
48. Jin,S. *et al*. (1998) Differential etoposide sensitivity of cells deficient in the Ku and DNA-PKcs components of the DNA-dependent protein kinase. *Carcinogenesis*, **19**, 965–971.
49. Errami,A. *et al*. (1996) Ku86 defines the genetic defect and restores X-ray resistance and V(D)J recombination to complementation group 5 hamster cell mutants. *Mol. Cell. Biol.*, **16**, 1519–1526.

50. Singleton,B.K. *et al*. (1997) Molecular and biochemical characterization of xrs mutants defective in Ku80. *Mol. Cell. Biol.*, **17**, 1264–1273.
51. Lees-Miller,S.P. *et al*. (1995) Absence of p350 subunit of DNA-activated protein kinase from a radiosensitive human cell line. *Science*, **267**, 1183–1185.
52. Zhao,Y. *et al*. (2006) Preclinical evaluation of a potent novel DNA-dependent protein kinase inhibitor NU7441. *Cancer Res.*, **66**, 5354–5362.
53. Xu,W. *et al*. (2000) Nitric oxide upregulates expression of DNA-PKcs to protect cells from DNA-damaging anti-tumour agents. *Nat. Cell Biol.*, **2**, 339–345.
54. Um,J.H. *et al*. (2004) Association of DNA-dependent protein kinase with hypoxia inducible factor-1 and its implication in resistance to anticancer drugs in hypoxic tumor cells. *Exp. Mol. Med.*, **36**, 233–242.
55. Ginis,I. *et al*. (2000) Hypoxia affects tumor cell invasiveness *in vitro*: the role of hypoxia-activated ligand HAL1/13 (Ku86 autoantigen). *Cancer Lett.*, **154**, 163–174.
56. Lynch,E.M. *et al*. (2001) Hypoxia-activated ligand HAL-1/13 is lupus autoantigen Ku80 and mediates lymphoid cell adhesion *in vitro*. *Am. J. Physiol. Cell Physiol.*, **280**, C897–C911.
57. Iyer,N.V. *et al*. (1998) Cellular and developmental control of O_2 homeostasis by hypoxia-inducible factor 1α. *Genes Dev.*, **12**, 149–162.
58. Welford,S.M. *et al*. (2006) HIF1α delays premature senescence through the activation of MIF. *Genes Dev.*, **20**, 3366–3371.
59. Le Bras,A. *et al*. (2007) HIF-2α specifically activates the VE-cadherin promoter independently of hypoxia and in synergy with Ets-1 through two essential ETS-binding sites. *Oncogene*, **26**, 7480–7489.
60. Zeng,L. *et al*. (2007) Hypoxia inducible factor-1 influences sensitivity to paclitaxel of human lung cancer cell lines under normoxic conditions. *Cancer Sci.*, **98**, 1394–1401.
61. Dominguez-Sola,D. *et al*. (2007) Non-transcriptional control of DNA replication by c-Myc. *Nature*, **448**, 445–451.
62. Huang,L.E. *et al*. (2007) Hypoxia-induced genetic instability—a calculated mechanism underlying tumor progression. *J. Mol. Med.*, **85**, 139–148.

Received June 17, 2008; revised September 24, 2008;
accepted September 28, 2008